JOURNAL OF MATERIALS SCIENCE **33** (1998) 5715–5729

Crack bridging and fibre pull-out in polyethylene fibre reinforced epoxy resins

P. I. GONZÁLEZ-CHI, R. J. YOUNG
Manchester Materials Science Centre, University of Manchester/UMIST, Grosvenor Street, Manchester M1 7HS, UK
E-mail: robert.young@umist.ac.uk

An investigation has been undertaken of the stress distributions in high-performance polyethylene fibres bridging cracks in model epoxy composites. The axial fibre stress has been determined from stress-induced Raman band shifts and the effect of fibre surface treatment has been followed using untreated and plasma-treated polyethylene fibres. It is found that when the specimen is cracked, the fibres do not break and stress is transmitted from the matrix to the fibre across the fibre/matrix interface. A debond propagates along the fibre/matrix interface accompanied by friction along the debonded interface. The axial stress distributions in the fibres can be analysed using a partial-debonding model based upon shear-lag theory and it is found that the maximum interfacial shear stress at the bond/debond transition is a function of the debond length. The debonding process has been modelled successfully in terms of the interfacial fracture energy-based criterion developed by Hsueh for the propagation of a debond along a fibre/matrix interface accompanied by constant friction along the interface.

Nomenclature

a	Debonded length ($0 \leq x \leq a$), Crack length (mode II)
E_c	Composite tensile modulus
E_f	Fibre tensile modulus
E_m	Matrix tensile modulus
G_m	Matrix shear modulus
G_i	Energy release rate for frictional debonding
L	Embedded length
m	Constant
n	Non-dimensional shear-lag parameter
r	Fibre radius
R	Radius of a cylindrical matrix shell around the fibre (Volume fraction parameter)
s	Fibre aspect ratio
U_e	Elastic strain energy in the fibre and matrix
U_s	Energy due to sliding at debonded interface
u_{deb}	Additional axial displacement due to debonding
V_f	r^2/R^2 = Fibre volume fraction
V_m	$1 - V_f$ = Matrix volume fraction
W	Work done by the applied stress due to interfacial debonding
w_f	Axial displacement in the fibre resulting from the axial stress
w_m	Axial displacement in the matrix resulting from the axial stress
x	Position along the fibre
μ	Frictional coefficient
σ_d	Stress for initial debonding (frictionless debonding)
σ_{fc}	Stress on the bonded region
σ_{fe}	Stress on the debonded region
σ_{fd}	Fibre tensile stress at the transition between debonded and bonded region
σ_{md}	Matrix tensile stress at the transition between bonded and debonded region
σ_0	Bridging stress on the fibre across the crack
σ_r	Residual stress
τ	Interfacial shear stress in the bonded region
τ_i	Interfacial shear stress in the debonded zone
τ_{max}	Maximum interfacial shear stress in the bonded region

1. Introduction

A number of experimental techniques such as single-fibre pull out [1, 2] and fragmentation [2, 3] have been developed to measure the adhesion between a rigid fibre and a composite matrix. Most of these techniques are based on the use of the interfacial shear stress (ISS) as the parameter to characterise the strength of the interface. Despite the popularity of this approach and the large quantity of experimental data that has been obtained, there have been suggestions that the ISS probably is not the critical factor that controls fibre-matrix debonding in composites [4–6]. Significant differences in the values of ISS are often encountered for similar experiments carried out by different groups of workers [7]. One reason for this is the difference in the nature of the micromechanical test methods employed. The loading configurations and the specimen geometries vary from test to test and therefore the stress fields induced are different. Also the analyses of these complex

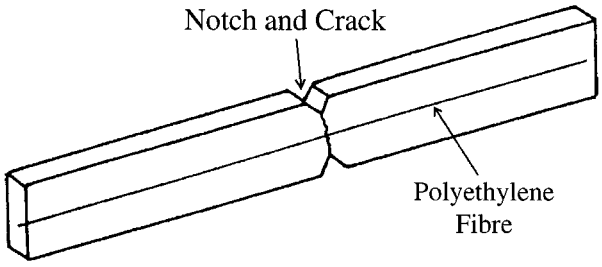

Figure 1 Schematic diagram of the single-fibre composite specimen showing the notch and crack.

stress states in the test-pieces are usually very simplistic [8–11] often being based upon shear-lag models and linear-elastic behaviour.

2. New test geometry

In this paper a different test geometry is proposed based on exploiting the difference in mechanical properties between a polyethylene (PE) fibre and an epoxy resin matrix. A resin bar containing a long single PE fibre is separated into two blocks by propagating a crack across the middle of the bar without breaking the fibre and the final result is two epoxy blocks bridged by a PE filament (Fig. 1). The fibre/matrix interface is then debonded by separating the two blocks. This geometry has a number of advantages over the fragmentation and pull-out tests for the PE/epoxy system. When the two blocks are separated, the stress is transmitted directly to the fibre through the interface because the fibre is the only link between the two blocks. This does not happen, for example, in the fragmentation test [2, 3], where the applied stress is distributed throughout the resin and then transmitted to the fibre through the interface. Another advantage of the new test method is that the resin blocks lack a meniscus at the point where the fibre enters the resin. Consequently problems encountered with the stress concentrations where the fibre enters the resin, that are characteristic of the single-fibre pull-out test [1, 2], are reduced.

The test can be considered essentially to be a double pull-out test, in which the interface is deformed directly. There is also better control of the debonding process due to the lack of the long free fibre length outside the resin block that is often employed in the conventional pull-out [1, 2]. The free fibre length in the double pull-out test is essentially the crack-opening displacement. Nevertheless, the precracking process introduces an extra complication. When the resin is deformed, the crack travels through the resin at high speed and when it reaches the fibre, part of the energy is dissipated by debonding the interface through the well-known Cook-Gordon mechanism [12, 13].

The proposed geometry in Fig. 1 is also a model for the crack-bridging process which is thought to be an important toughening mechanism in fibre-reinforced composites [20] where there is bridging of matrix cracks by fibres which debond from and slip fictionally against the matrix [14, 15] as shown in Fig. 2. The conventional geometries used most widely to study this mechanism are unidirectional systems with arrays of continuous

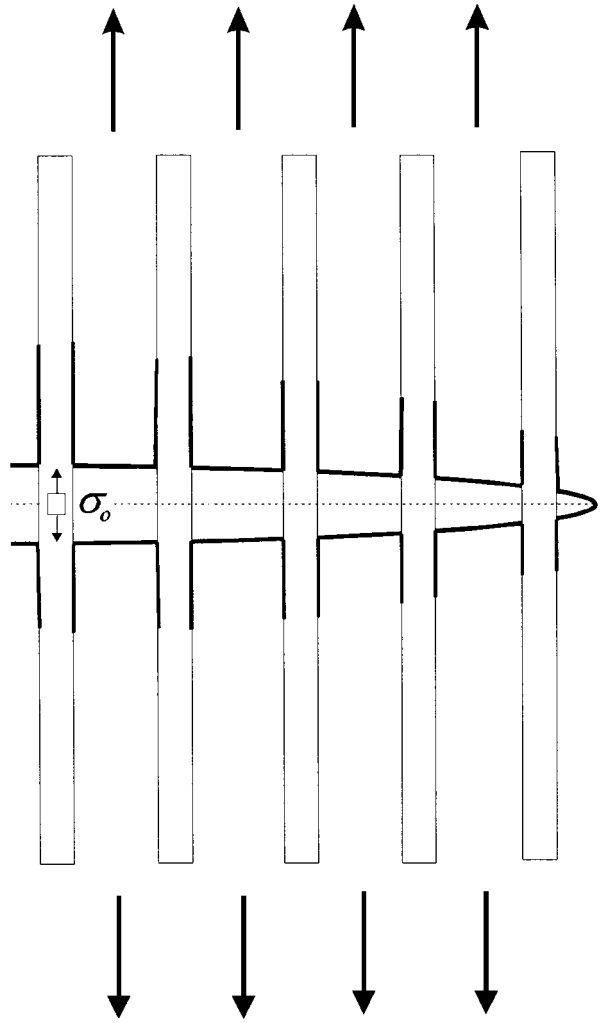

Figure 2 Schematic diagram showing a matrix crack bridged by a number of aligned fibres [20]. The debonded regions along the fibres are represented by thick lines.

fibres aligned along the direction of tensile loading. A mode I crack is traditionally propagated through the matrix in a direction perpendicular to the reinforcing fibres. Debonding is the basic precursor to the bridge-formation stage. The primary crack (mode I) deflects along the matrix/fibre interface, progressively transferring the applied load from the matrix to the fibre as the walls separate. The deflected crack (mode II) develops a large component of shear as it spreads along the fibre-matrix interface and at a critical displacement or stress, the fibre ruptures (or debonds fully). The debonded fibre begins to slide out against the frictional restraint of the matrix walls, exerting a closure stress.

The geometry used in this present study to estimate the strength of the interface between a PE fibre and an epoxy resin (crack pull-out) is shown in Fig. 3 and contains several important differences from the conventional crack-bridging geometry. The technique requires the fracture of a resin bar with a single fibre embedded in its centre into two blocks without breaking the fibre. This is done by propagating a crack (mode I) through the centre of the bar perpendicular to the fibre. As the blocks are separated, stress is transmitted to the fibre through the interface but the fibre is strong enough to resist the applied stress level without failing. Also, its

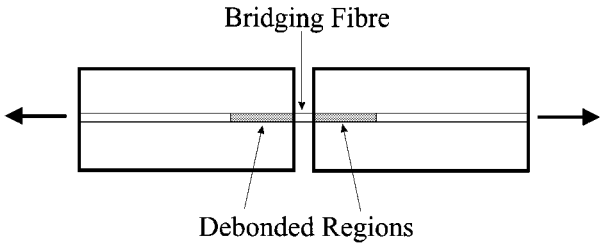

Figure 3 Schematic diagram of the single-fibre composite specimen showing a crack-bridging fibre and the debonded regions.

embedded length is long enough to make pull out practically impossible. On the other hand, the interface is weak enough to fail preferentially. The final effect is a relatively-stable debonding front (mode II crack) travelling along the fibre-matrix interface with no fibre failure or frictional pull-out and no direct load on the matrix.

The main advantage of this geometry is a better control of the debonding process. The deformation of the fibre in the resin and movement of the debonding front can easily be detected using Raman spectroscopy by following the peak position of the 1127 cm^{-1} Raman band of the polyethylene (PE) fibre. This band corresponds to the symmetric C–C stretching mode and shifts linearly with the applied stress [16]. The rate of shift, better known as Raman Stress Sensitivity Factor (SSF) can be used to convert the band position of an embedded fibre into axial fibre stress [17]. This means that by obtaining spectra from a fibre inside a composite, it is possible to measure not only the stress transfer along fibre but also the extent of debonding. In other words it is possible to detect the length of the mode II crack propagating along the fibre surface and also the axial stress distribution in the fibre. Both parameters can be used in the energy approach for the analysis of the strength of the fibre/matrix interface [18–20]. This has been suggested as probably a better approach than strength-based criteria based upon the shear-lag analysis [21–24].

3. Partial-debonding theory

The shear-lag theory of Cox [25] was modified by Piggott [26] for the single-fibre pullout test to develop a partial-debonding theory in which the fibre/matrix interface is divided in two regions. In the first region, the fibre is debonded and the stress changes linearly with position along the fibre such that the ISS is constant. In the second region, where the fibre is still fully-bonded to the resin, the deformation is linear elastic and the axial fibre stress and ISS decay in an exponential manner.

This model can easily be extended to crack bridging by considering each block as a single pull-out test (Fig. 3) where the stress and the ISS in the debonded region are given by

$$\sigma_{\mathrm{fe}} = \sigma_0 - \frac{2\tau_i x}{r} \tag{1}$$

$$\tau_i = -\mu\sigma_r \tag{2}$$

In the case of the elastic region, the equations that describe the stress and ISS along the fibre are

$$\sigma_{\mathrm{fc}} = \sigma_{\mathrm{fd}}\left[\frac{\sinh\left(\frac{n(L-x)}{r}\right)}{\sinh(nsm)}\right] \tag{3}$$

$$\tau = \frac{n\sigma_{\mathrm{fd}}}{2}\left[\frac{\cosh\left(\frac{n(L-x)}{r}\right)}{\sinh(nsm)}\right] \tag{4}$$

with

$$\sigma_{\mathrm{fd}} = \sigma_0 - \frac{2\tau_i(1-m)L}{r} \tag{5}$$

$$n^2 = \frac{2G_{\mathrm{m}}}{E_{\mathrm{f}}\ln(R/r)} \tag{6}$$

and

$$s = \frac{L}{r} \tag{7}$$

These equations can be used to fit the experimentally-determined variation of axial stress with position along a fibre obtained by Raman spectroscopy.

4. Energy-based criterion

The energy criterion presented by Hsueh [20] for a unidirectional composite loaded in tension in the fibre direction can be summarised as follows. A crack propagates perpendicular to the loading direction and is bridged by intact fibres (Fig. 2). The model uses the representative volume element shown in Fig. 4 which contains a single fibre bridging the crack with a section debonded partially.

The debonding criterion can be obtained from the energy balance condition such that:

$$\mathrm{d}W = \mathrm{d}U_{\mathrm{e}} + \mathrm{d}U_{\mathrm{s}} + \mathrm{d}G_i \tag{8}$$

(a) U_{e} has two components, the elastic energy for the bonded section (U_{eb}) and that for the debonded section (U_{ed}). In the first case, the elastic energy for the fibre in the matrix can be calculated from the elastic strain density of the system (from the linear elastic response of the materials). If the debonded region advances a distance dx, the bonded region is also reduced by a length dx and a volume $\pi R^2\mathrm{d}a$, hence

$$\mathrm{d}U_{\mathrm{eb}} = -\frac{\pi R^2}{2}\left(\frac{V_{\mathrm{f}}\sigma_{\mathrm{f}}^2}{E_{\mathrm{f}}} + \frac{V_{\mathrm{m}}\sigma_{\mathrm{m}}^2}{E_{\mathrm{m}}}\right)\mathrm{d}a \tag{9}$$

where

$$\sigma_{\mathrm{f}} = \frac{V_{\mathrm{f}}E_{\mathrm{f}}\sigma_0}{E_{\mathrm{c}}}, \quad \sigma_{\mathrm{m}} = \frac{V_{\mathrm{f}}E_{\mathrm{m}}\sigma_0}{E_{\mathrm{c}}} \tag{10}$$

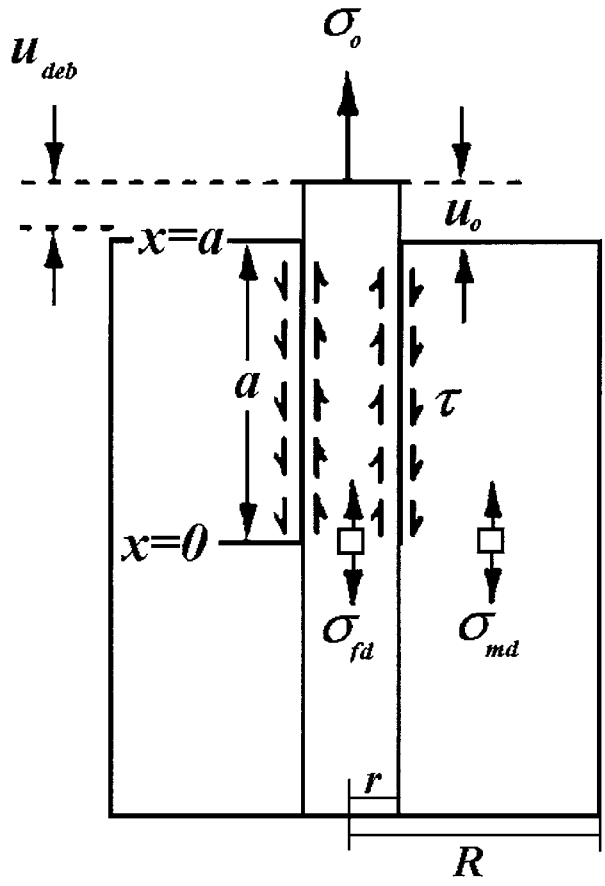

Figure 4 A representative volume element for the energy-based criterion showing a loaded fibre bridging a crack.

Substituting into Equation 9 gives

$$\mathrm{d}U_{\mathrm{eb}} = \frac{-\pi R^2 V_{\mathrm{f}} \sigma_0^2 \,\mathrm{d}a}{2E_{\mathrm{c}}} \tag{11}$$

In the debonded region, the elastic strain density is given by

$$U_{\mathrm{ed}} = \frac{\pi R^2}{2} \int_0^a \left(\frac{V_{\mathrm{f}} \sigma_{\mathrm{f}}^2}{E_{\mathrm{f}}} + \frac{V_{\mathrm{m}} \sigma_{\mathrm{m}}^2}{E_{\mathrm{m}}} \right) \mathrm{d}x \tag{12}$$

From a force balance on the interface between the tensile and shear stresses (assuming τ_i is constant)

$$\sigma_{\mathrm{f}} = \sigma_{\mathrm{fd}} - \frac{x(\sigma_0 - \sigma_{\mathrm{fd}})}{a}, \quad \sigma_{\mathrm{m}} = \left(1 - \frac{x}{a}\right)\sigma_{\mathrm{md}} \tag{13}$$

and

$$\sigma_{\mathrm{fd}} = \sigma_0 - \frac{2a\tau_i}{r}, \quad \sigma_{\mathrm{md}} = \frac{2aV_{\mathrm{f}}\tau_i}{rV_{\mathrm{m}}} \tag{14}$$

Substituting for σ_{f} and σ_{m}, integrating Equation 12 and differentiating with respect to a gives

$$\mathrm{d}U_{\mathrm{ed}} = \frac{\pi r^2}{2E_{\mathrm{f}}} \left(\sigma_0^2 - \frac{4a\tau_i\sigma_0}{r} + \frac{4a^2\tau_i^2 E_{\mathrm{c}}}{r^2 V_{\mathrm{m}} E_{\mathrm{m}}} \right)^2 \mathrm{d}a \tag{15}$$

Combining Equations 11 and 15 leads to

$$\mathrm{d}U_{\mathrm{e}} = \mathrm{d}U_{\mathrm{eb}} + \mathrm{d}U_{\mathrm{ed}} = \frac{\pi r^2 V_{\mathrm{m}} E_{\mathrm{m}}}{2E_{\mathrm{f}}E_{\mathrm{c}}} \left(\sigma_0 - \frac{2a\tau_i E_{\mathrm{c}}}{rV_{\mathrm{m}}E_{\mathrm{m}}} \right)^2 \mathrm{d}a \tag{16}$$

(b) U_{s}. This sliding energy is dissipated due to the relative displacement between the fibre and matrix at constant τ_i. Hence

$$U_{\mathrm{s}} = 2\pi r \int_0^a \tau_i (w_{\mathrm{f}} - w_{\mathrm{m}}) \,\mathrm{d}x \tag{17}$$

where w_{f} and w_{m} are the axial displacements in the fibre and the matrix resulting from the axial stress (Equations 13). They are given by the integration of the function that defines the axial deformation

$$w_{\mathrm{f}} = \frac{x\sigma_{\mathrm{fd}}}{E_{\mathrm{f}}} + \frac{x^2(\sigma_0 - \sigma_{\mathrm{fd}})}{2aE_{\mathrm{f}}}, \quad w_{\mathrm{m}} = \left(x - \frac{x^2}{2a} \right) \frac{\sigma_{\mathrm{md}}}{E_{\mathrm{m}}} \tag{18}$$

Substituting in Equation 17, integrating and differentiating U_{s} with respect of a:

$$\mathrm{d}U_{\mathrm{s}} = 2\pi r\tau \left(\frac{a\sigma_0}{E_{\mathrm{f}}} - \frac{2a^2\tau_i E_{\mathrm{c}}}{rV_{\mathrm{m}}E_{\mathrm{f}}E_{\mathrm{m}}} \right) \mathrm{d}a \tag{19}$$

(c) W. The work done due to interfacial debonding with a bridging stress, σ_0, is

$$W = \pi r^2 \sigma_0 u_{\mathrm{deb}} \tag{20}$$

where u_{deb} is given by

$$u_{\mathrm{deb}} = \frac{aV_{\mathrm{m}}E_{\mathrm{m}}\sigma_0}{E_{\mathrm{f}}E_{\mathrm{c}}} - \frac{a^2\tau_i}{rE_{\mathrm{f}}} \tag{21}$$

Differentiating Equations 20 and 21 with respect to a and re-combining leads to

$$\mathrm{d}W = \pi r^2 \sigma_0 \left(\frac{V_{\mathrm{m}}E_{\mathrm{m}}\sigma_0}{E_{\mathrm{f}}E_{\mathrm{c}}} - \frac{2a\tau_i}{rE_{\mathrm{f}}} \right) \mathrm{d}a \tag{22}$$

(d) G_i. When the debonded length advances $\mathrm{d}a$, the debonded interface area is $2\pi r\,\mathrm{d}a$. The change in the interfacial energy is

$$\mathrm{d}G_i = 2\pi r G_i \,\mathrm{d}a \tag{23}$$

(e) The energy balance is obtained by substituting Equations 16, 19, 22 and 23 into 8:

$$\sigma_0 = 2\left(\frac{E_{\mathrm{f}}E_{\mathrm{c}}G_i}{rV_{\mathrm{m}}E_{\mathrm{m}}} \right)^{1/2} + \frac{2a\tau_i E_{\mathrm{c}}}{rV_{\mathrm{m}}E_{\mathrm{m}}} \tag{24}$$

This equation defines the relationship between the bridging stress, σ_0, the interface energy, G_i, and the frictional debond length a.

The value of σ_d can be obtained from Equation 24 by letting $a = 0$ (or $\tau_i = 0$) so that

$$\sigma_d = 2\left(\frac{E_f E_c G_i}{r V_m E_m}\right)^{1/2} \quad (25)$$

Combining Equations 24 and 25, the debonded length, a, becomes:

$$a = \frac{r V_m E_m (\sigma_0 - \sigma_d)}{2 E_c \tau_i} \quad (26)$$

Substitution of Equations 25 and 26 into Equation 21 yields:

$$u_{deb} = \frac{r V_m^2 E_m^2 \sigma_0^2}{4 E_f E_c^2 \tau} - \frac{V_m E_m G_i}{E_c \tau_i} \quad (27)$$

Hsueh [20] pointed out that the above solution was identical to his previous results [23] in which interfacial debonding was assumed to occur when the mismatch in the axial strain between the fibre and matrix reached a critical value. Moreover, the mismatch criterion was found [20] to bear the same physical meaning as strength-based criteria for debond propagation [23].

5. Experimental

5.1. Materials

The Epoxy resin used for the composites was Ciba-Geigy HY5052/LY5052 cured for at least 7 days at room temperature, 22 ± 2 °C. The matrix mechanical properties were: modulus, 3.45 ± 0.1 GPa, elongation at break, $1.9 \pm 0.4\%$ and shear yield strength, 41.8 ± 2 MPa [27].

Two commercial grades of PE fibre were supplied by Allied-Signal, Petersburg, USA: Spectra 1000 (US) and Spectra 1000 with Plasma Treatment (TS – the exact treatment is proprietary). The fibre diameters are 34.2 ± 7.4 μm for US and 32.4 ± 5.4 μm for TS. The manufacturer describes these fibres as having a modulus of 170 GPa, a tensile strength of 3 GPa and a maximum elongation of 2.7% (at a strain rate of 0.02 s^{-1}).

5.2. Raman spectroscopy

The Raman Spectrometer used was a Renishaw 1000 Raman Imaging Microscope [28] fitted with a 30 mW HeNe laser (633 nm) model 127-25 from Spectra-Physics. The laser power on the sample surface was controlled in the range of 0.1–10 mW using an attenuation filter wheel. In the case of the PE fibres, an intensity of about 1.4 mW was used. The spectrometer microscope is a modified Olympus optical microscope model BH2 fitted with 20× and 50× objective lenses. One of the main advantages of the Renishaw spectrometer is that can be operated as a confocal optical system [29], which allows the laser beam to be focused precisely on the sample to a small elliptical spot of 2×1 μm (major axes) with a 2 μm depth (50× objective). The monochromator has a single diffraction grating with a spectral resolution of 1 cm^{-1}. The intensity of the Raman bands in materials with a high degree of molecular orientation are very sensitive to the polarisation direction of the laser, which is the case of the high-performance PE fibres was parallel to the axis of the fibres. A highly-sensitive, Peltier-cooled CCD detector [28] was used as a photon counting system for the recording the spectra. Another advantage of the Renishaw System is its high sensitivity; however, careful control of the alignment of the laser beam, the slit adjustment and the CCD chip area need for good results.

5.3. Specimen preparation

5.3.1. Single fibre deformation

Individual fibres were fixed to rectangular paper window frames with a gauge length of 100 mm. The fibres were first fixed to the frame ends using sticky tape. They were then glued to one side to the frame ends with epoxy resin which was allowed to set overnight at room temperature. The next day, the opposite sides of the frame ends were glued in the same way. The samples were stored in an atmosphere-controlled room (23 ± 1 °C and $50\% \pm 2\%$ humidity) for at least one week after being glued to the frames, in order to allow the resin to cure completely.

5.3.2. Composite specimens

Eight single filaments were suspended in a paper frame with a central area of 200×200 mm and a thickness of 2 mm. The frame was then fixed to a picture-frame mould placing the fibres at 2 mm from the mould bottom. About 60 g of the resin pre-mixed with 38% of hardener, degassed by vacuum was poured into the mould and allowed to set overnight at room temperature. The plates were all stored in an atmosphere-controlled room (23 ± 1 °C and $50\% \pm 2\%$ humidity) until they were ready to be tested. Once the plates were cured fully, 16 bars were cut from each one. The bar dimensions were $10 \times 3 \times 80$ mm containing a single filament along the central region. Then two opposing notches with a 60° angle and 2 mm depth were machined in the centre of each bar. The next step was to pre-crack the specimens which was done at least 4 weeks after moulding to ensure full curing. One of the notches was sharpened using a razor blade, and then the crack was propagated by carefully tapping the bar. The crack was not allowed to reach the opposite notch and stopped very close to it.

5.4. Test procedure

5.4.1. Single fibre deformation

The fibre frame (100 mm gauge length) was fixed to a weight-driven rig. One end of the rig had a small platform where weights of ~ 2 g could be placed. At the opposite end a 1 N load cell was attached and the whole system was placed under the Raman microscope. The frame edges were cut and the laser beam focused on a central point on the fibre. A spectrum was taken using a 4 s exposure, then a 2 g weight was placed on the rig platform and a time of 15 s was allowed

for the fibre to respond to the stress. When the load cell reading reached a steady value, which was recorded, the next spectrum was taken. This procedure was repeated steadily at intervals of 2 g up to a maximum load of ~ 48 g.

5.4.2. Composite specimens

Each specimen was cemented to a straining rig using cyanoacrylate glue and placed on the microscope stage of the Raman spectrometer. The initial mapping was performed by taking Raman spectra using 5 s exposure along the section of the embedded fibre between the two notches, before cracking the bar. The pre-cracked specimen was then similarly mapped along the fibre, from one side of the crack, through the crack and onto the opposite side. Finally, the bar was cracked completely by moving the micrometer rig to separate the two resin blocks. The fibre surface was mapped again from one block, across the crack plane to the opposite block. The micrometer was used to increase the gap between the two blocks and the interface mapping was performed again. This whole procedure was repeated until the debonding front reached zones out of the range of the microscope stage. The debonding front travelled several mm further along the fibre interface each time the blocks were separated, requiring an increasing mapping time to cover the debonded region fully. The Raman band position ($\Delta\nu$) was transformed into stress (σ) from the calibrated band shift [30] and then plotted against distance x along the fibre.

6. Results and discussion

6.1. Fibre deformation

Fig. 5a shows the Raman spectrum for the Spectra gel-spun polyethylene fibre in the region 1000–1500 cm^{-1}. It can be seen that there are four well-defined Raman bands with the one due to C–C symmetric stretching at 1127 cm^{-1} being the strongest. It was found that this band shifted to lower wavenumber under a tensile stress as shown in Fig. 5b which shows the band position at three strain levels.

The shift of the band position was calibrated against applied stress for the two Spectra fibres as shown in Fig. 6.The dependence of the peak position upon stress is shown in Fig. 6a for six nominally-identical US fibres. It can be seen that there is a clear shift to lower wavenumber although there is a range of slopes due probably to variations in fibre diameter and difficulty in achieving good adhesion of the US fibre to the testing rig. Similar data are shown in Fig. 6b for six nominally-identical TS fibres. In this case there is rather less variability in slope due to better adhesion of the fibre. The mean rates of Raman bands shift per unit stress, $d\Delta\nu/d\sigma$, for the two fibres determined from Fig. 6 were 5.9 ± 1.1 cm^{-1}/GPa for the US fibre and 5.6 ± 0.4 cm^{-1}/GPa for the TS fibre.

6.2. Partial-debonding theory

Because of the test procedure, two different stages in the debonding process need to be defined. Initially, the pre-cracking of the resin bar promotes the propagation of a crack (which eventually divides the bar into two blocks). As this crack reaches the fibre, the fibre/matrix interface becomes partially debonded. The second stage occurs when the two resin blocks are separated, forcing the debonding front to propagate along the fibre/matrix interface. Both mechanisms are analyzed separately in the following sections and compared for US and TS fibres. Their respective profiles of axial fibre stress are fitted to cubic spline curves for clarity.

6.2.1. Pre-cracked bar

The two fibre stress distributions presented in Fig. 7 are for the US and TS fibres and each plot shows two profiles. The first one corresponds to the stress in the fibre before the crack is propagated through the resin bar (no crack) and in both cases the data points are scattered around zero stress showing that there is no residual fibre stress for this cold-cured system. The second profile (0 μm) represents the stress distribution along the fibre for the unstressed pre-cracked resin bar and is characteristic of partial debonding [31]. When the crack reaches the fibre, it is deflected along the interface because, for this system, the interface is relatively weak and the fibre is strong as shown was schematically in Fig. 2. The stress rises along the fibre as the crack is approached and it peaks, then falls and becomes slightly compressive across the crack plane. The fall in stress is due to a reverse sliding process taking place during crack closure [24, 31].

The debonded region is longer for the US fibre (Fig. 7a) and shows a lower maximum stress than for the TS fibre (Fig. 7b). This difference in behaviour is due to the better adhesion of the TS fibre to the epoxy resin matrix producing stronger resistance to debonding along the fibre/matrix interface.

6.2.2. Fully-cracked bar

Fig. 8 shows the stress profiles for US and TS fibres after the epoxy bar was fully cracked and the two halves of the specimen separated. Each plot presents three distributions which correspond to stress profiles generated on the fibre surface as the gap between the two resin blocks was increased. Both sets of profiles show approximately the same maximum value of stress (~ 0.6 GPa). Nevertheless, the shape of the profiles are very different. The US fibre profiles show an approximately triangular distribution of stress, whereas the profiles for the TS fibre are more trapezoidal. Again, the US fibre (Fig. 8a) has broader debonded region than the TS fibre (Fig. 8b), due to its inferior adhesion to the matrix.

6.2.3. Modelling

The shear lag theory approach developed by Piggott [26] for the single-fibre pull-out test was used to model the Raman stress profiles and subsequently to calculate the ISS distributions. Fig. 9a shows the axial stress distributions for the US fibre, fitted to the partial-debonding model and Fig. 9b gives the corresponding

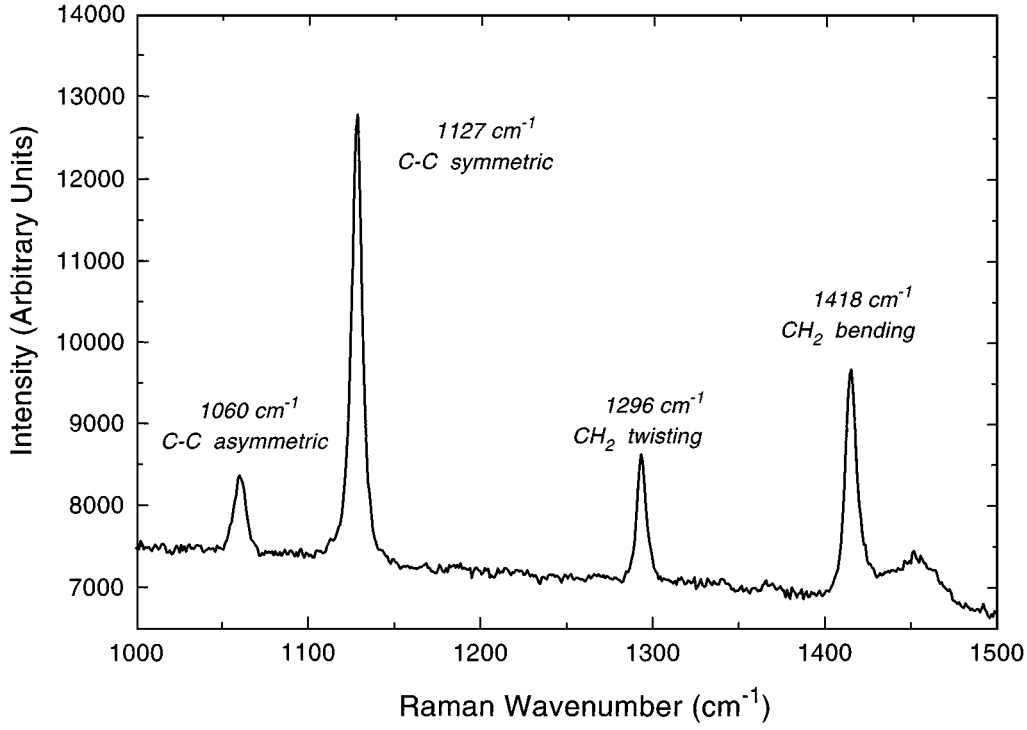

(a)

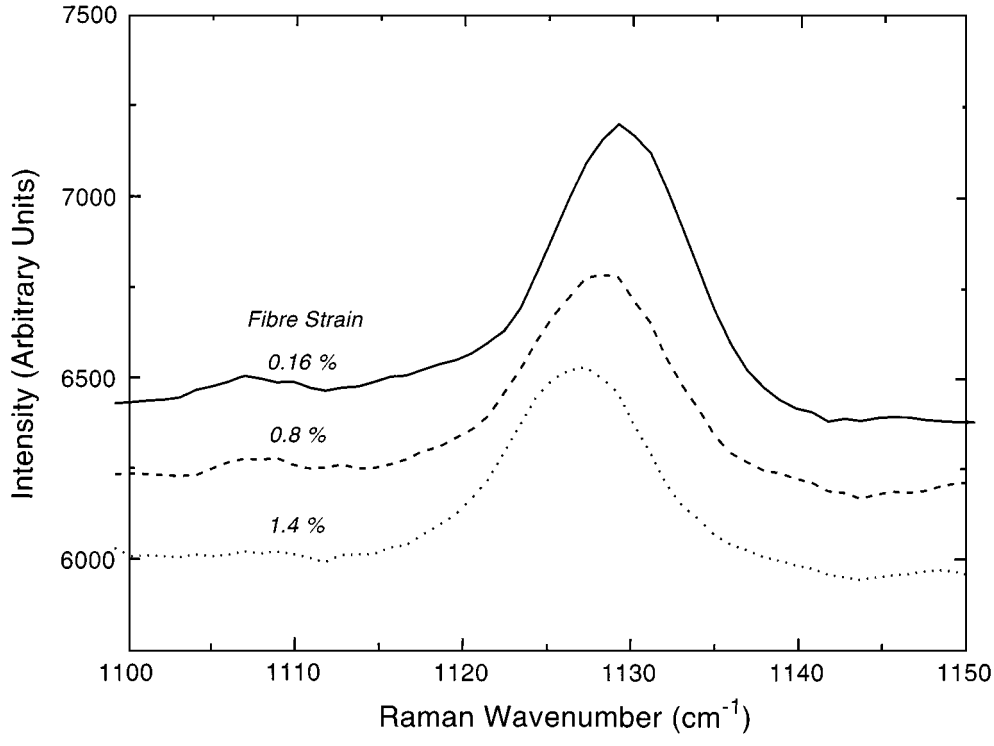

(b)

Figure 5 (a) Raman spectrum in the region 1000–1500 cm^{-1} for a single filament of the spectra 1000 polyethylene fibre. (b) Strain-induced shift of the 1127 cm^{-1} Raman band.

ISS distribution. All the profiles in each block show two regions. The first is a debonded one, near to the crack plane with several linear sections each with a constant ISS ranging from 3 to 5 MPa, i.e. the frictional ISS. The second region corresponds to a bonded fibre situation, in which the materials behave elastically and there is good bonding. There is a maximum, τ_{max}, in ISS at the transition point between the two regions and this transition point moves away from the crack plane as the gap between the blocks is increased. Simultaneously, the maximum ISS increases.

It is interesting to observe from Fig. 9a the initial stages of reloading the specimen after precracking. When the crack-opening displacement (COD) is increased to 115 μm, the debonded front does not travel further inwards, the only change observed is that the fibre takes up the stress across the crack plane in the debonded region. The initial opening of the crack does

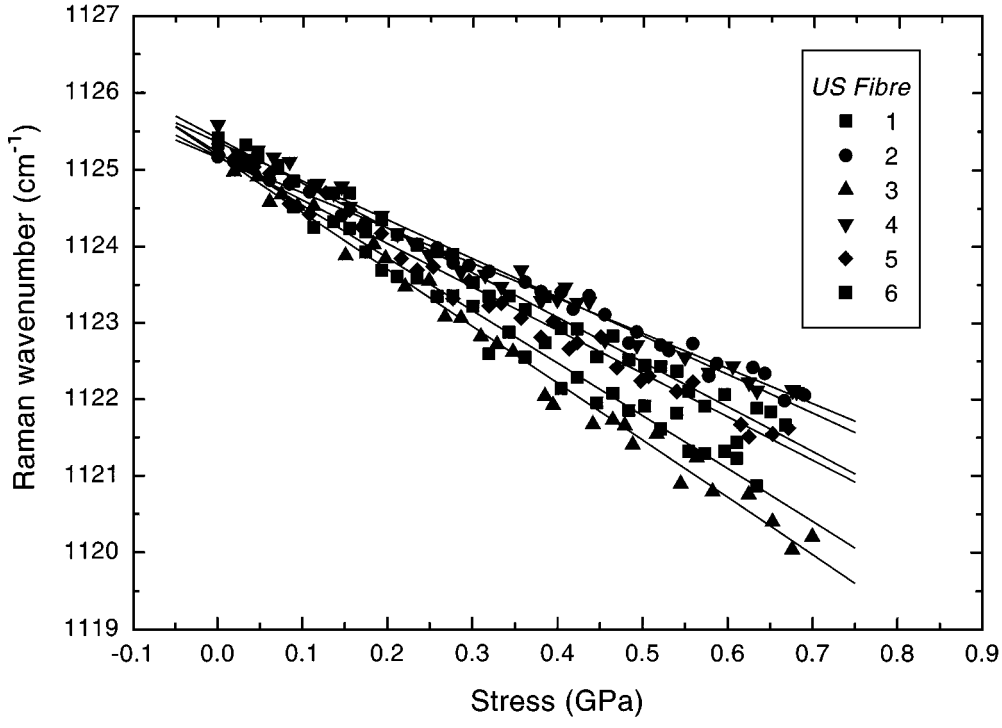

(a)

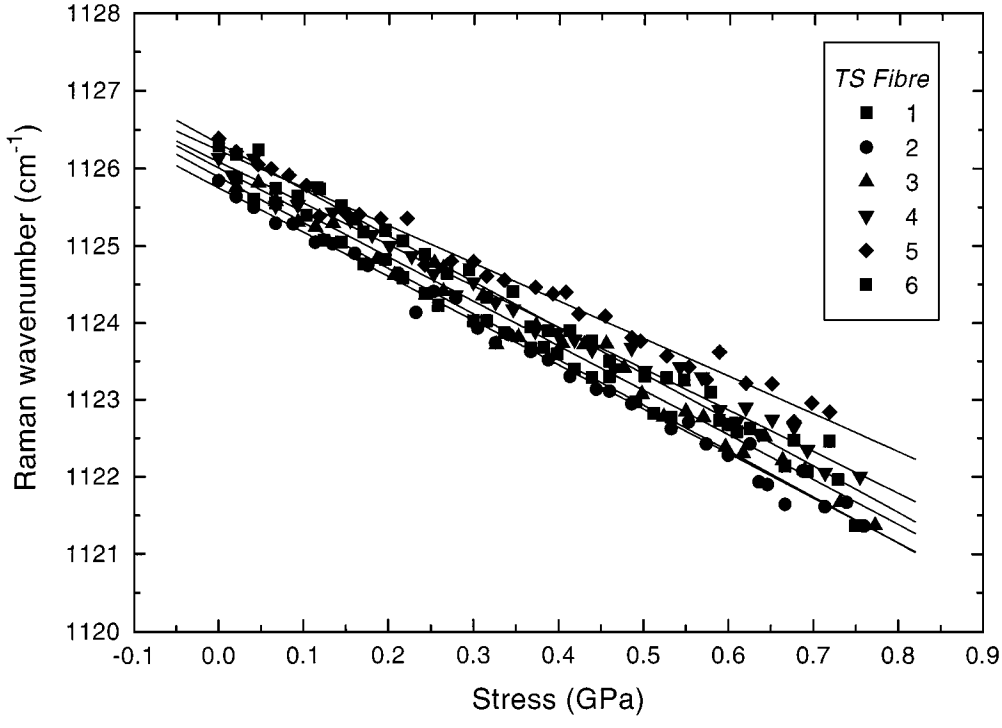

(b)

Figure 6 Dependence of the peak positions of the 1127 cm^{-1} Raman band upon stress for 6 nominally-identical filaments. (a) Untreated US fibre and (b) plasma-treated TS fibre.

not lead to extra debonding of the interface, it only causes reverse sliding at the interface. Further increases in the COD to 210 and 300 μm cause both an increase in fibre stress across the crack plane and the debonded regions to increase in length.

Fig. 10 shows the stress distributions fitted to the partial-debonding model, and the corresponding ISS distributions for TS fibre. The general behaviour of this fibre is similar to that of the US fibre and the main difference is in the levels of ISS reached. The plasma treatment of the fibre surface improves the adhesion to the resin, making the interface more resistant to failure. The maximum ISS in the elastic regions ranges from 2 to 8 MPa, which is about 3 times higher than for the US fibre (Fig. 9). Also, the debonded region extends no more that 10 mm either side of the crack plane for a COD of 300 μm compared with 15 mm for the US fibre.

It was explained earlier that it is possible to analyse the failure of the fibre/matrix interface in terms of either

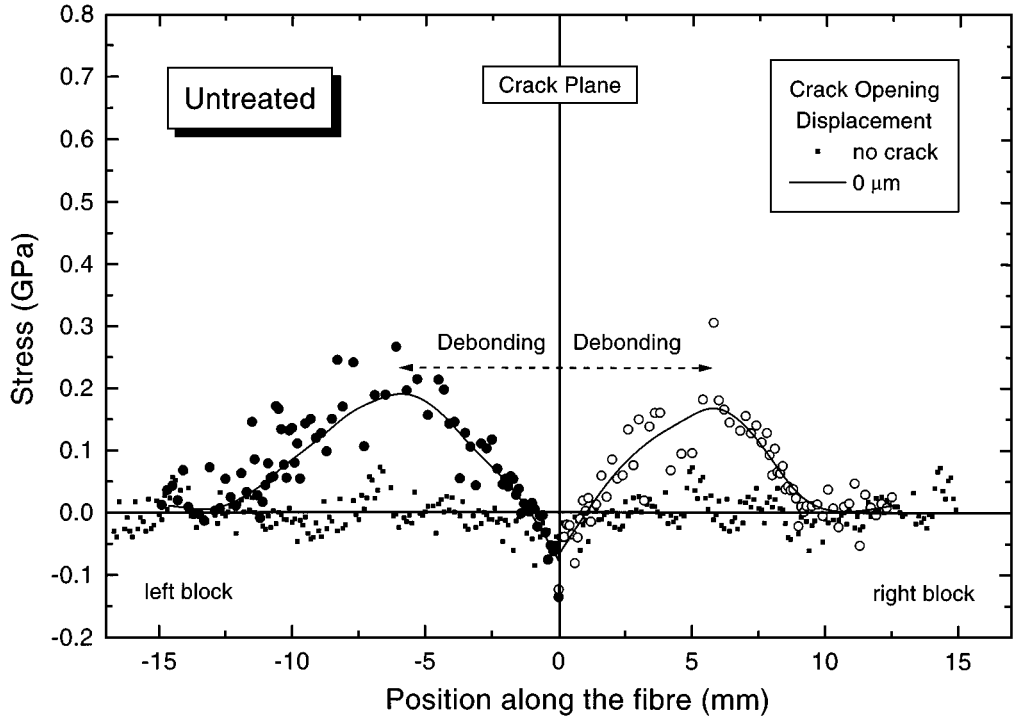

(a)

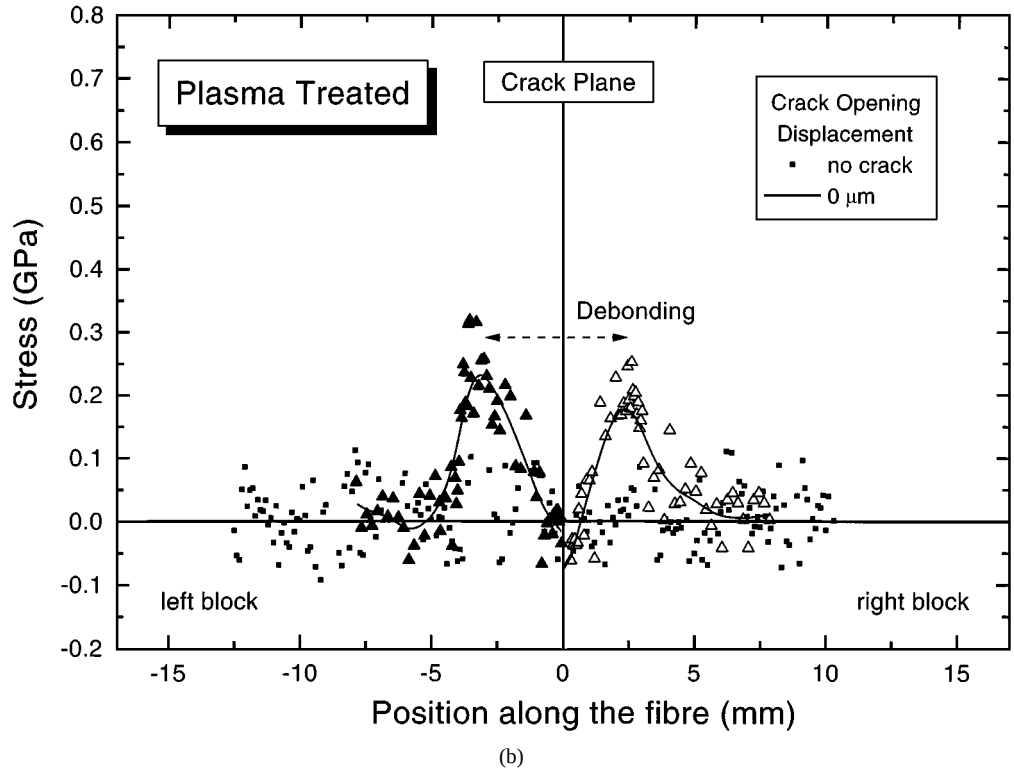

(b)

Figure 7 Derived variations of axial fibre stress along single PE filaments in the precracked model composite specimens. (a) Untreated US fibre and (b) plasma-treated TS fibre.

a stress-based or an energy-based criterion. The data in Figs 9 and 10 allow a critical analysis of the failure criteria to be undertaken. The values of maximum ISS, τ_{max}, as a function of debond length taken from Figs 9b and 10b are plotted in Fig. 11 and it can be seen that for both the US and TS fibre the maximum ISS increases with increasing debond length. This means that the ISS at the transition from a bonded to a debonded region appears to be a function of the length of the debond. It implies therefore that the assumption that debonding is controlled by the shear stress at the interface is not appropriate for this polyethylene-fibre/epoxy system.

It should be noted that a stress-based criterion appeared to work for the pull-out of aramid fibres from an epoxy resin block [1] where the fibre/matrix interface was significantly stronger and debond lengths were relatively small (>1 mm). Interfacial failure appeared to take place at an approximately constant ISS. The difference in the behaviour of the PE/epoxy system may be due to the weakness of the interface and the length of

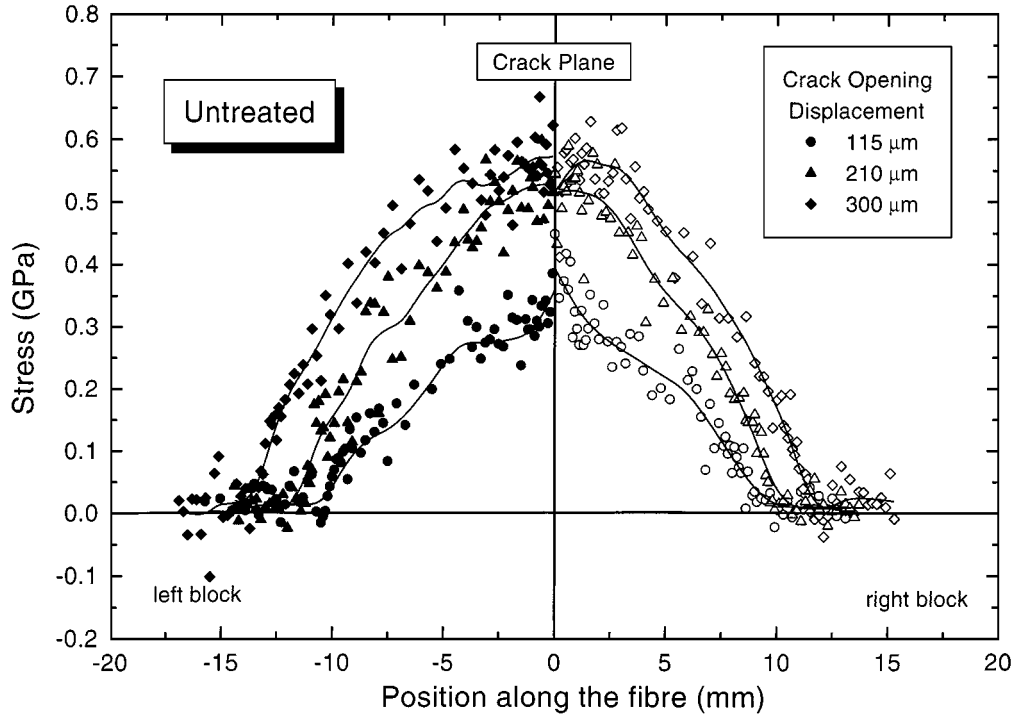

(a)

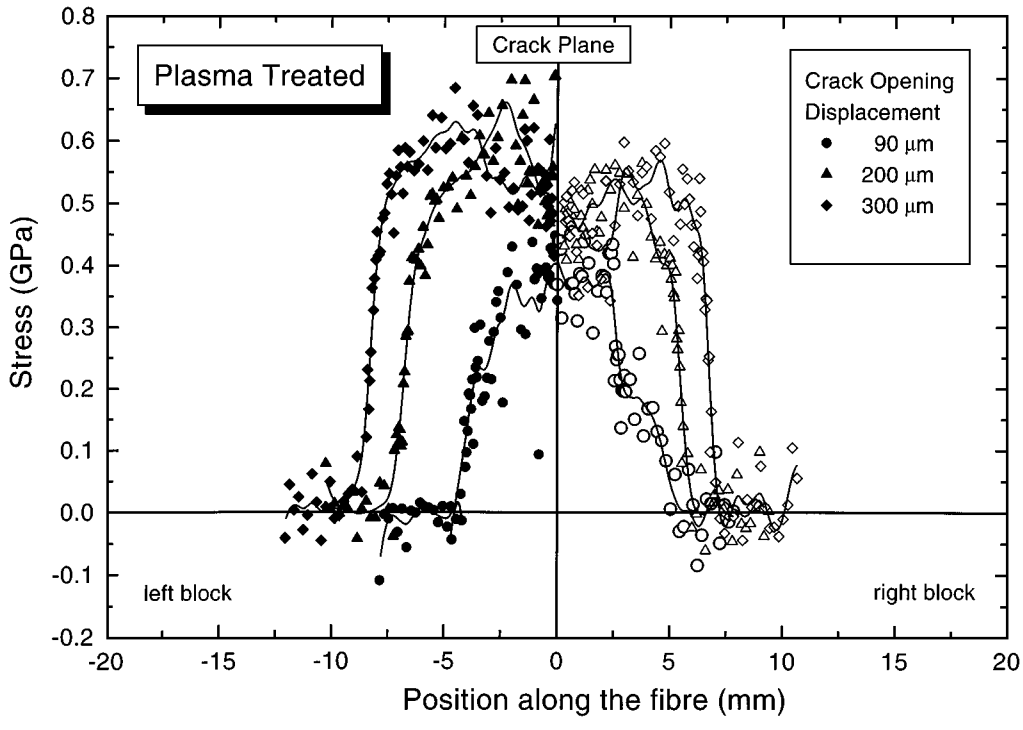

(b)

Figure 8 Derived variations of axial fibre stress along single PE filaments bridging the crack in the loaded model composite specimens. (a) Untreated US fibre and (b) plasma-treated TS fibre.

the debonded regions allowing a more critical analysis of the failure criterion.

6.3. Energy-based criterion

The stress applied to the sample was increased in a "fixed-grip" fashion and under such conditions, the elastic energy in the system was used to propagate the interfacial crack. In the previous section, the stress profiles were fitted to a partial debonding model which allows detection of the transition point between the bonded and the debonded region. If it is assumed that the tip of the mode II crack is located at this transition point, the crack length (a) can be considered as the distance from the block edge to the transition point along the fibre.

Equation 24 relates the stress in the bridging fibre on a crack (σ_0) to the energy available to propagate the mode II crack along the fibre interface (G_i). This equation was originally developed for a high

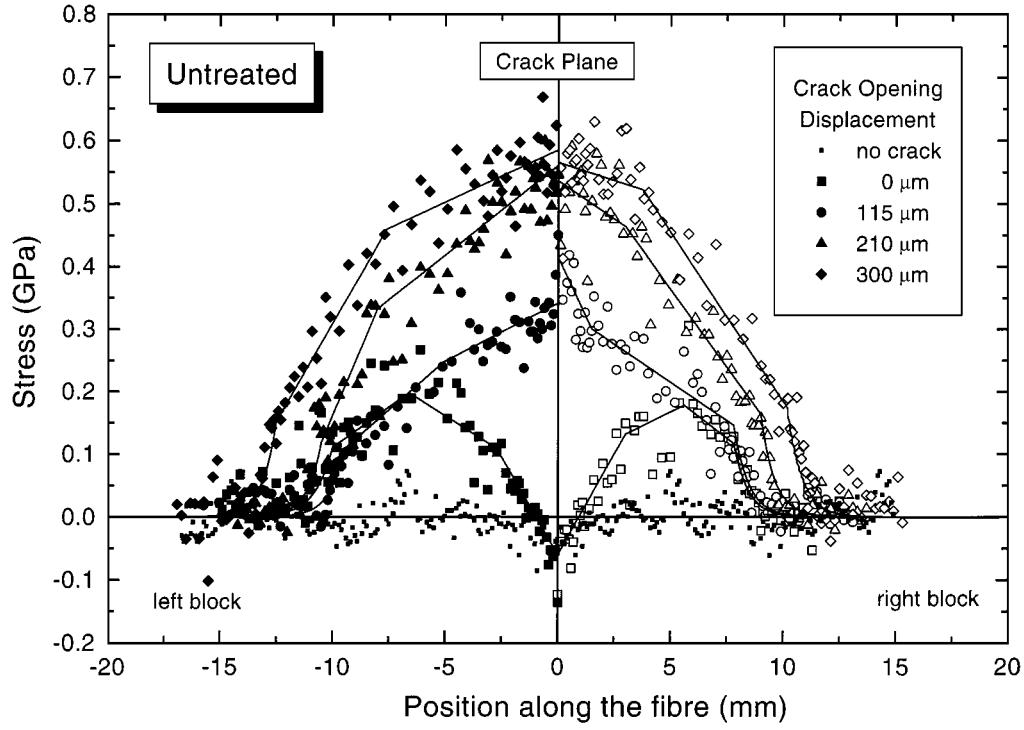

(a)

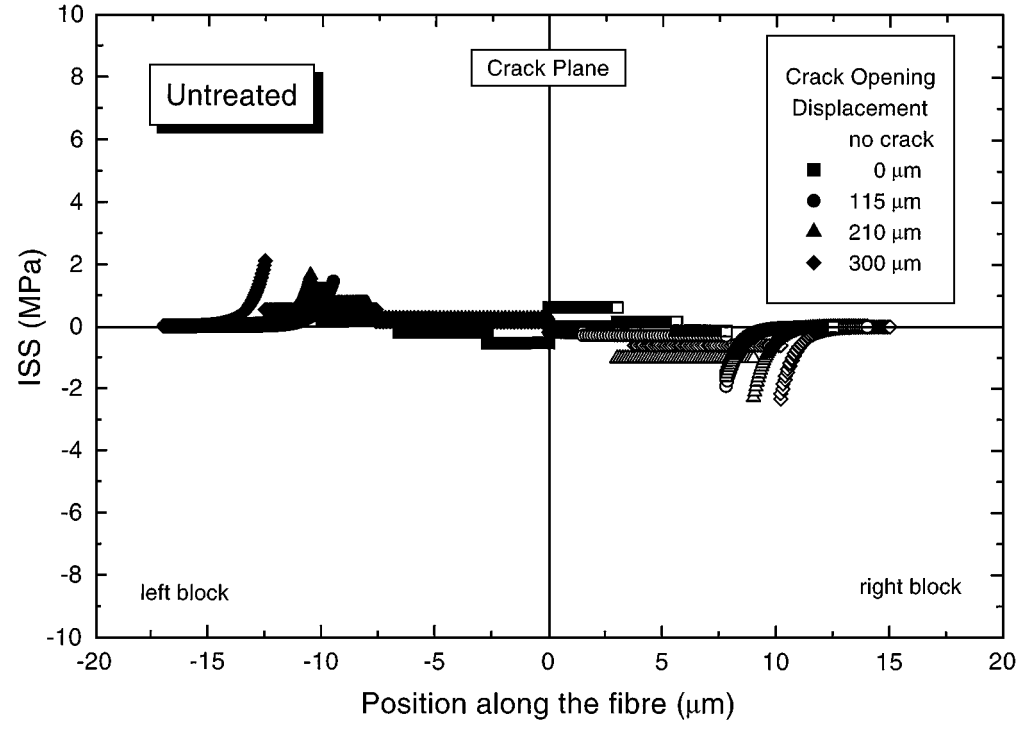

(b)

Figure 9 (a) Variations of axial fibre stress along a single untreated US fibres bridging a crack in a loaded model composite specimen at different levels of COD. The solid lines are fits of the data points to the partial-debonding theory. (b) Derived variations of ISS along the fibre from the data in (a).

volume-fraction composite [20] but it can be easily adapted to our model composite by making the following assumptions: $E_c \approx E_m$ and $V_m \approx 1$. This transforms Equation 24 into

$$\sigma_0 = 2\left(\frac{E_f G_i}{r}\right)^{1/2} + \frac{2a\tau_i}{r} \qquad (28)$$

Equation 28 predicts a linear relationship between the bridging stress (σ_0) and the product of the crack length (debonded length) and the interfacial shear stress in the debonded region ($a\tau_i$). G_i can be calculated from the intersection of this line with the y-axis since E_f and r are known.

The Raman stress profiles presented in Figs 9 and 10 were used to derive σ_0. The partial debonding theory [3, 26] assumes a linear stress distribution along the debonded region on the interface but due to the loading of the specimen in a "fixed grip" mode, part of the debonded fibre relaxes sometimes showing several

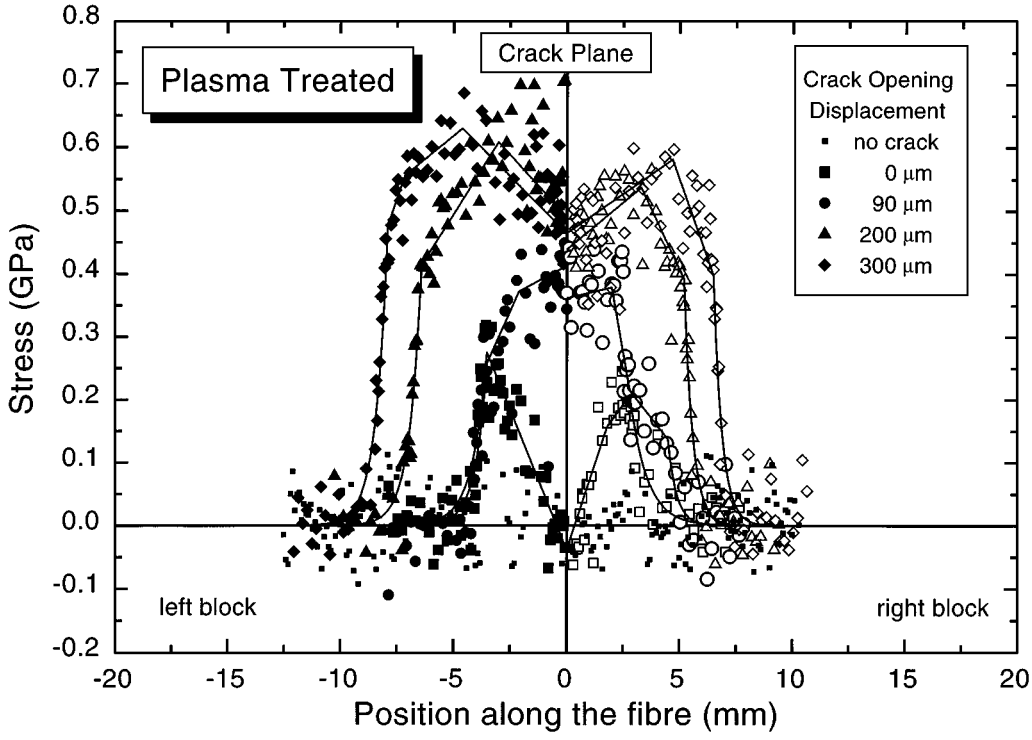

(a)

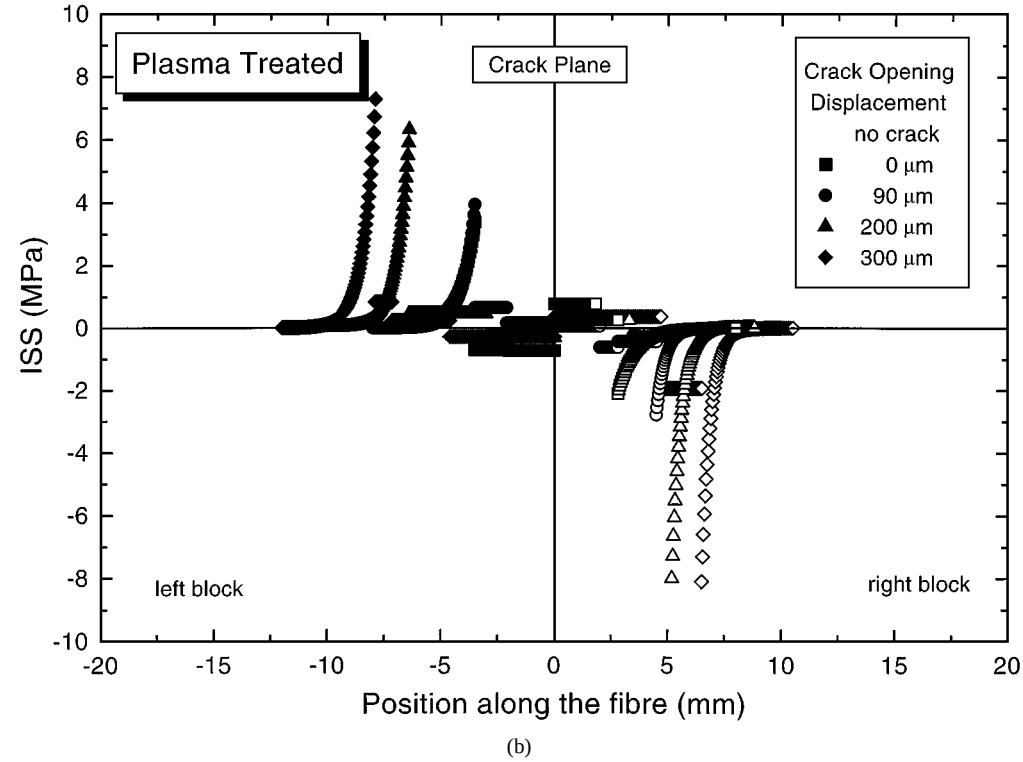

(b)

Figure 10 (a) Variations of axial fibre stress along a single plasma-treated TS fibres bridging a crack in a loaded model composite specimen at different levels of COD. The solid lines are fits of the data points to the partial-debonding theory. (b) Derived variations of ISS along the fibre from the data in (a).

different linear regions [29]. The value of σ_0 was determined by extrapolating the stress distribution in the debonded region closest to the transition point to the y-axis as shown in Fig. 12.

Fig. 13 shows a plot of σ_0 as a function of $a\tau_i$ for the US and TS fibres according to Equation 28 and it can be seen that the data fall upon straight lines. The values of a and τ_i were taken from Figs 9 and 10 and are presented in Table I. The values of σ_0 calculated from the Raman stress profiles are presented in Table II along with the values of G_i determined from Fig. 13. It can be seen that the energy required to propagate a mode II crack along the interface between the Untreated Spectra 1000 fibre (US) and the epoxy resin (0.15 J m^{-2}) is about 60 times lower than the energy of 9.6 J m^{-2} required to propagate interface failure between the resin and the Plasma Treated Spectra 1000 fibre (TS). This demonstrates clearly that the surface

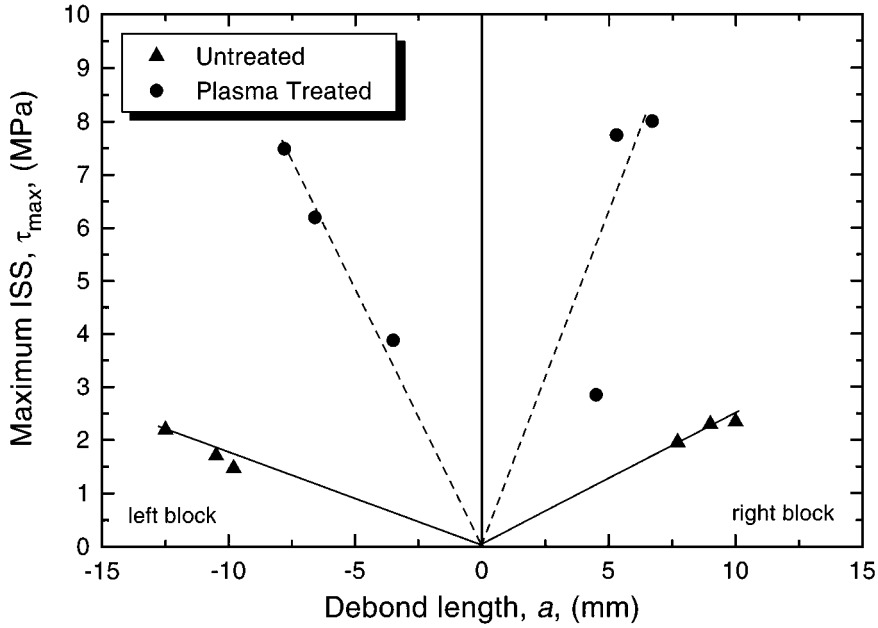

Figure 11 Dependence of the maximum interfacial stress upon debond length. Data taken from Figs 9b and 10b.

TABLE I Debonding parameters for untreated (US) and plasma treated (TS) fibres

	Block	Gap (μm)	a (mm)	τ_i (MPa)	τ_{max} (MPa)
US	Left	0	−10	0.24	1.22
		115	−9.5	0.27	1.46
		210	−10.5	0.73	1.70
		300	−12.5	0.54	2.19
	Right	0	7.5	−0.12	−1.66
		115	7.8	−0.29	−1.95
		210	9	−1.02	−2.29
		300	10	−0.61	−2.33
TS	Left	0	−3.5	−0.77	3.48
		90	−3.5	0.64	3.87
		200	−6.4	0.45	6.19
		300	−7.9	0.82	7.48
	Right	0	2.8	0.39	−2.06
		90	4.5	−0.44	−2.84
		200	5.2	−0.33	−7.74
		300	6.5	−2.01	−8.00

TABLE II Bridging stress and fracture energy for PE/epoxy composite

	Block	Gap (μm)	σ_0 (GPa)	G_i (J/m^2)
US	Left	115	0.40	0.15 ± 0.02
		210	1.02	
		300	0.94	
	Right	115	0.34	
		210	0.61	
		300	0.72	
TS	Left	90	0.54	9.6 ± 0.20
		200	0.78	
		300	0.76	
	Right	90	0.79	
		200	0.79	
		300	1.06	

The values of σ_0 were determined using the extrapolation procedure shown in Fig. 12.

treatment improves the bonding of the fibre with the matrix and that the behaviour can be modelled using an energy-based criterion which discriminates well between the two different surface treatments.

7. Conclusions

Raman Spectroscopy has been shown to be an excellent method of following the micromechanics of deformation of fibre-reinforced composites, which for the PE/Epoxy system is particularly interesting due to the ease of producing debonding at a weak fibre/matrix interface. In the case of the crack pull-out geometry, the accuracy of detecting the way in which the debonding front travels along the embedded fibre has allowed a link to be made between the derived fibre stress distributions and fracture mechanics.

The crack pull-out geometry was shown to have several advantages over conventional single-fibre composite and pull-out geometries. The stress is applied more efficiently to the interface for the crack pull-out geometry. There is no stress concentration at the point where the fibre enters the resin and the geometry emulates crack-bridging in a real composite very well allowing the debonding process to be followed clearly.

The Raman stress profiles were fitted using a partial debonding model considering the geometry as a double pull-out test. It was found that controlled debonding at the fibre/matrix interface could be obtained as the two halves of the specimen were separated and that the fibre stress distribution could be modelled accurately using the partial debonding model. Although it was shown that the interfacial shear stress at the bond/debond transition was significantly higher for the TS fibre than that for the US fibre due to the plasma surface treatment, in both cases it was found that the maximum value of ISS for progressive debonding was a function of debond length.

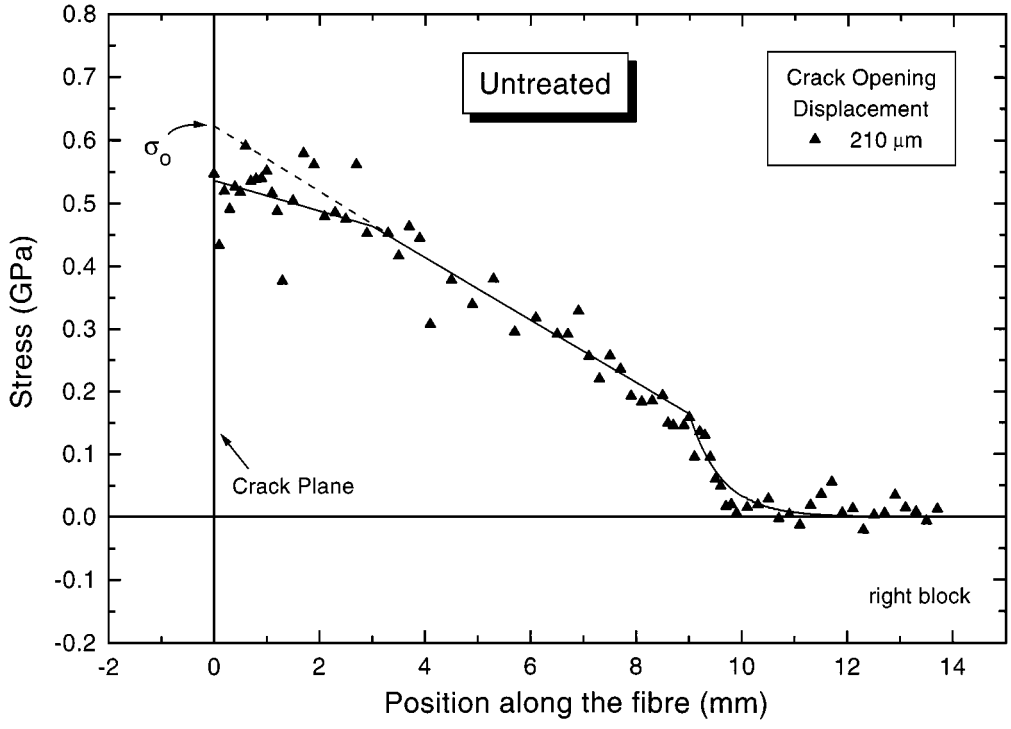

(a)

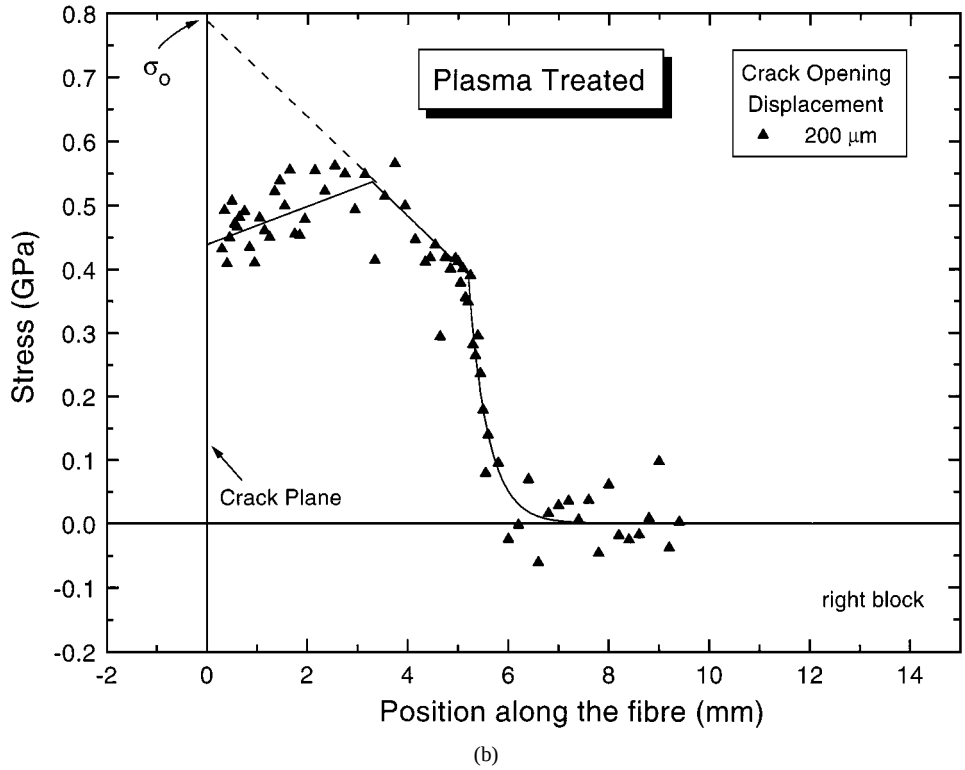

(b)

Figure 12 Determination of the crack bridging stress. (a) Untreated Spectra 1000 (US) and (b) plasma-treated Spectra 1000 (TS).

It appears that the energy-based criterion used in the model presented by Hsueh [20] gives a better explanation of the failure criterion for debonding the fibres in terms of the interfacial fracture energy, G_i, than models based upon the ISS. In the case of the US fibre, the parameter G_i was found to be 0.15 ± 0.2 J m^2 and for TS fibre was found to be 9.6 ± 0.02 J/m^2. Hence the surface treatment on the fibre improves its interaction with the resin resulting in a stronger interface which requires over 60 times more energy to cause debonding than for the untreated fibre.

Acknowledgements

P. I. G-Ch. would like to thank to Consejo Nacional de Ciencia y Technologia (CONACyT) of México for financial support and R. J. Y. is grateful to the Royal Society for the Wolfson Research Professorship and

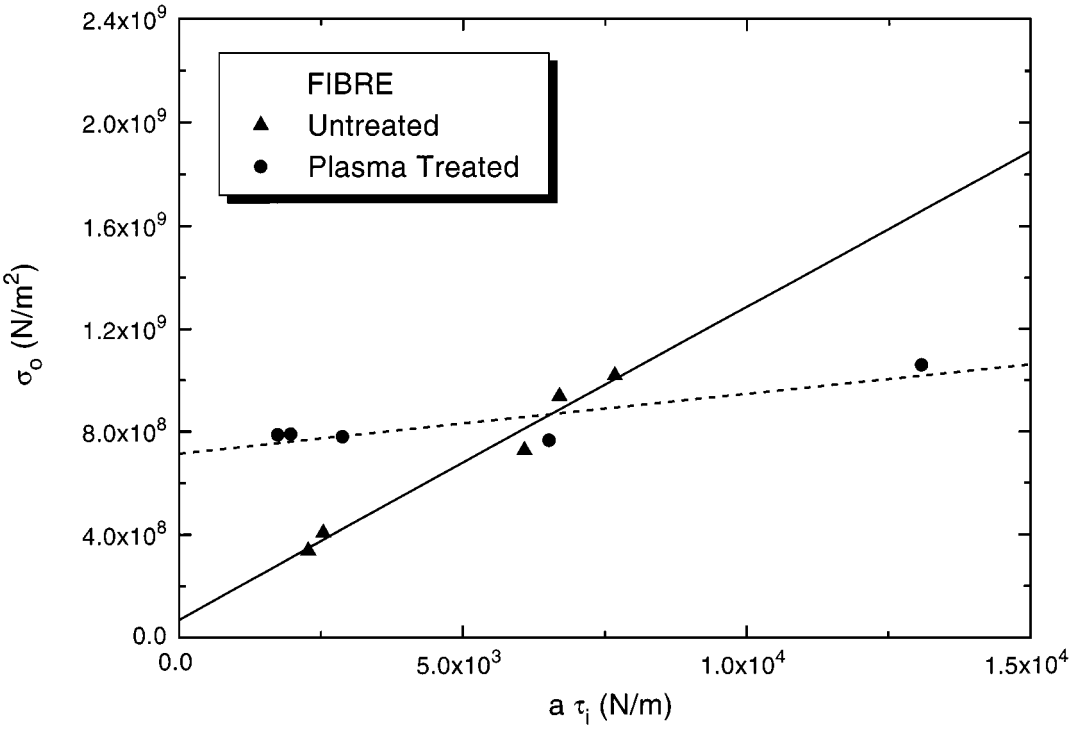

Figure 13 Variation of the crack bridging stress, σ_0 with $a\tau_i$ according to the energy-based failure criterion, for the untreated Spectra 1000 (US) and plasma-treated Spectra 1000 (TS) fibres (the lines are least square fits of the data points).

EPSRC for the support to the overall programme of Raman spectroscopy to the analysis of fibre and composite deformation. The authors are also grateful to Dr C.-H. Hsueh of Oak Ridge National Laboratory for valuable discussions.

References

1. D. J. BANNISTER, M. C. ANDREWS, A. CERVENKA and R. J. YOUNG, *Compos. Sci. Technol.* **53** (1995) 411.
2. R. J. YOUNG, Y.-L. HUANG, X. GU and R. J. DAY, *Plastics, Rubber and Composites: Processing and Applications* **23** (1995) 11.
3. Y. HUANG and R. J. YOUNG, *Composites* **26** (1995) 541.
4. K. KENDALL, *J. Mater. Sci.* **11** (1976) 638.
5. R. J. SCHEER and J. NAIRN, *Compos. Eng.* **2** (1992) 641.
6. A. T. DIBENEDETTO, *Compos. Sci. Technol.* **42** (1991) 103.
7. M. J. PITKETHLY, J. P. FAVRE, U. GAUR, J. JAKUBOWSKI, S. F. MUDRICH, D. L. CALDWELL, L. T. DRZAL, M. NARDIN, H. D. WAGNER, L. DILANDRO, A. HAMPE, J. P. ARMISTEAD, M. DESAEGER and I. VERPOEST, *ibid.* **48** (1993) 205.
8. L. T. DRZAL and M. MADHUKAR, *J. Mater. Sci.* **28** (1993) 569.
9. B. MILLER, P. MURI and L. REBENFELD, *Compos. Sci. Technol.* **28** (1987) 17.
10. M. R. PIGGOTT, P. S. CHUA and D. ANDISON, *Polym. Compos.* **6** (1985) 242.
11. B. LAWN, "Fracture of Brittle Solids," 2nd edition (Cambridge University Press, UK, 1993).
12. J. COOK and J. E. GORDON, *Proc. Roy. Soc. London* **A282** (1964) 508.
13. A. KELLY and N. H. MACMILLAN, "Strong Solids," 2nd edition (Clarendon Press, Oxford, 1986).
14. A. G. EVANS and R. M. MCMEEKING, *Acta Metallurgica* **34** (1986) 2435.
15. P. F. BECHER, C-H. HSUEH, P. ANGELINI and T. N. TIEGS, *J. Amer. Ceram. Soc.* **71** (1988) 1050.
16. W. F. WONG and R. J. YOUNG, *J. Mater. Sci.* **29** (1994) 510.
17. P. I. GONZÁLEZ-CHI, Deformation micromechanics in polyethylene-epoxy fibre-reinforced composites, Ph.D. thesis, UMIST, 1997.
18. Y-W. MAI, *Mater. Forum* **11** (1988) 232.
19. C. GURNEY and J. HUNT, *Proc. Roy. Soc. London* **A299** (1967) 508.
20. C. H. HSUEH, *Acta Metallurgica et Materialia* **44** (1996) 2211.
21. P. LAWRENCE, *Mater. Sci. and Eng.* **7** (1972) 1.
22. C-H. HSUEH, *ibid.* **A123** (1990) 1.
23. B. BUDIANSKY, A. G. EVANS and J. W. HUTCHINSON, *Int. J. Solid Structures* **32** (1995) 315.
24. C. H. HSUEH, *J. Mater. Sci.* **30** (1995) 1781.
25. H. L. COX, *British J. Appl. Phys.* **3** (1952) 72.
26. M. R. PIGGOTT, *Compos. Sci. Technol.* **30** (1987) 295.
27. M. C. ANDREWS, Stress transfer in arimid/epoxy model composites, Ph.D. thesis, University of Manchester Institute of Science and Technology (UMIST), 1994.
28. Renishaw Raman Microscope User Guide for Systems 1000, 2000 and 3000 Microscopes, Renishaw plc, UK, 1992.
29. R. J. MEIER and B. J. KIP, *Microbeam Analysis* **3** (1994) 61.
30. C. GALIOTIS, R. J. YOUNG, P. H. J. YEUNG and D. N. BATCHELDER, *J. Mater. Sci.* **19** (1984) 3640.
31. J. A. BENNETT and R. J. YOUNG, *Compos. Sci. Technol.* **57** (1997) 945.

Received 31 August
and accepted 18 September 1998